OPEN BIOLOGY

Planar cell polarity in the larval epidermis of Drosophila and the role of microtubules

Note: The following files were submitted by the author for peer review, but cannot be converted to PDF. You must view these files (e.g. movies) online.

Movie 1.avi
Movie 2.avi

SCHOLARONE™
Manuscripts

Author-supplied statements

Relevant information will appear here if provided.

Ethics

Does your article include research that required ethical approval or permits?:
This article does not present research with ethical considerations

Statement (if applicable):
CUST_IF_YES_ETHICS :No data available.

Data

It is a condition of publication that data, code and materials supporting your paper are made publicly available. Does your paper present new data?:
Yes

Statement (if applicable):
Data used in figures 4, 8, S1, S4-6 can be obtained from the University of Cambridge Open Access repository (https://doi.org/10.17863/CAM.53667)

Conflict of interest

I/We declare we have no competing interests

Statement (if applicable):
CUST_STATE_CONFLICT :No data available.

Authors' contributions

This paper has multiple authors and our individual contributions were as below

Statement (if applicable):
SP and KN carried out genetic crosses and image capture, participated in data analysis, participated in the design of the study and revised the manuscript; JC carried out statistical analyses and critically revised the manuscript; SP, PAL and JC conceived and designed the study. PAL wrote the manuscript. All authors gave final approval for publication and agree to be held accountable for the work performed therein.

Planar cell polarity in the larval epidermis of *Drosophila* and the role of microtubules

Stefano Pietra[1], KangBo Ng[1,2], Peter A. Lawrence[1,3], José Casal[1,3]

[1] Department of Zoology, University of Cambridge, Downing Street, Cambridge CB2 3EJ, United Kingdom

[2] Current Address: The Francis Crick Institute, 1 Midland Road, London NW1 1AT and Institute for the Physics of Living Systems, University College London, London, United Kingdom

[3] Authors for correspondence (pal38@cam.ac.uk, jec85@cam.ac.uk)

Keywords: Planar Cell Polarity, *Drosophila*, larval epidermis, microtubules, protocadherins, *dachsous*, *fat*, *ovo*, *dachs*

ABSTRACT

We investigate planar cell polarity (PCP) in the *Drosophila* larval epidermis. The intricate pattern of denticles depends on only one system of PCP, the Dachsous/Fat system. Dachsous molecules in one cell bind to Fat molecules in a neighbour cell to make intercellular bridges. The disposition and orientation of these Dachsous-Fat bridges allows each cell to compare two neighbours and point its denticles towards the neighbour with the most Dachsous. Measurements of the amount of Dachsous reveal a peak at the back of the anterior compartment of each segment. Localisation of Dachs and orientation of ectopic denticles help reveal the polarity of every cell. We discuss whether these findings support our gradient model of Dachsous activity. Several groups have proposed that Dachsous and Fat fix the direction of PCP via oriented microtubules that transport PCP proteins to one side of the cell. We test this proposition in the larval cells and find that most microtubules grow perpendicularly to the axis of PCP. We find no meaningful bias in the polarity of microtubules aligned close to that axis. We also reexamine published data from the pupal abdomen and find no evidence supporting the hypothesis that microtubular orientation draws the arrow of PCP.

INTRODUCTION

As cells construct embryos and organs they need access to vectorial information that informs them, for example, which way to migrate, divide, extend axons and orient protrusions such as hairs. Cells in epithelia may produce oriented structures such as hairs or cilia and these are coordinated, pointing or beating in a particular orientation. This kind of polarity is known as planar cell polarity (PCP). In *Drosophila* there are (at least) two conserved genetic systems that generate PCP. Both systems rely on the formation of intercellular bridges made by transmembrane proteins containing cadherin repeats, these interact via their extracellular domains. The Dachsous/Fat (Ds/Ft) system depends on heterodimers of the protocadherins Ds and Ft while the Starry Night/Frizzled system relies on asymmetric homodimers of Starry Night (reviewed in [**1-6**]). Most developmental models can be tricky to study because both PCP systems operate at once and both have separate but confounding inputs into the orientation of bristles, etc. However, here we investigate the later stage larvae in which PCP depends entirely on the Ds/Ft system [**7-9**] whose mechanism is quite well understood. Ds molecules in one cell bind to Ft molecules in a neighbour cell to make intercellular bridges. Experiments argue that, using the disposition and orientation of Ds-Ft bridges, each cell compares the Ds activity of those two of its neighbours that lie in the relevant axis and points its denticles towards the neighbour with the ***higher*** Ds activity. Ds activity is thus an important component of the model: the activity of Ds in a cell defines its ability to bind to Ft in its neighbouring cell, that activity depending on at least three factors; the levels of Ds expression, the levels of Ft expression and the activity of Four-jointed (Fj). Fj is a Golgi-resident kinase that phosphorylates both Ds and Ft, reducing the activity of the former while increasing the activity of the latter [**10-12**].

The system has an additional property: because of the interdependence of membrane bound Ds and Ft in neighbouring cells, the polarity of one cell can affect the polarity of its neighbours and that polarity can be propagated to the next neighbour [**7, 13, 14**]. Thus, in these several ways the landscape of Ds activity in a field of cells is translated into the individual polarities of the cells

68 (see [5] for further explanation). More recently, we have, via experiments and

69 observations, developed a model that explains the quite complex pattern of

70 denticle polarities in the larval abdominal segment [15].

A model: the ventral epidermis of the *Drosophila* larva

72 Each segment of the larva is divided by cell lineage into an anterior (A) and a

73 posterior (P) compartment. In the adult abdomen, the A and P compartments are

74 thought to be approximately coextensive with opposing gradients of Ds activity

75 [16] and if such gradients were present in the larva then they could explain most

76 of the denticle polarities. However, in the larva, in addition to the normal

77 denticulated cells, there are three interspersed rows of muscle attachment cells

78 [15, 17, 18] and our experiments suggest that two of these three rows have

79 exceptionally low Ds activity which can affect the polarity of neighbouring cells

80 (**figure 1**, [15, 17]). At this point we are not clear how much the final pattern is

81 determined by pervasive gradients of Ds activity or how much by these local

82 effects of the muscle attachment cells plus propagation.

83   One outstanding difficulty in applying present models to the whole segment

84 is that more than half the cells do not make denticles and their polarities are not

85 known. In this paper we have solved that difficulty by measuring the molecular

86 polarities of these uncharted cells in two complementary and different ways and

87 this allows us to extend model-building to the entire segment. With the same

88 purpose we have also measured the amount of Ds expression in each

89 intercellular junction across the entire segment.

90   Depending on the pattern of Ds activity, individual cells will acquire

91 different numbers of Ds-Ft and Ft-Ds heterodimers at opposite cell faces.

92 Generally this difference will explain the polarity of the whole cell, however,

93 sometimes and depending on the disposition of neighbouring cells, two regions

94 of a single cell can have opposing polarities [17]. To explain this phenomenon it

95 has been argued that polarity of individual cells or parts of cells would depend

96 on local "conduits" that run between opposing cell faces to mediate their

97 comparison. In this paper we reinvestigate these multipolar cells in an

98 experimental situation.

99   There is some evidence that suggests that these conduits acting within the

100   Ds/Ft system could be microtubules and might polarise the cell by orienting the

101   intracellular transport of molecules and vesicles [**19, 20**]. Indeed Harumoto et al

102   reported that, in one particular region of the pupal wing, the majority of

103   microtubules are aligned near-parallel with the axis and direction of PCP (the

104   direction of PCP is defined by the orientation of hairs) and, when growing, they

105   show a small but statistically significant "bias" in polarity [**20**]. By bias we mean

106   a net difference between the number of microtubules growing within a particular

107   angle interval and the number of microtubules growing 180 degrees away; for

108   instance we might see more microtubules growing distally, ie in the same

109   direction as the hairs, than in the opposite direction. Harumoto et al therefore

110   proposed that, in general, the Ds/Ft system controls the orientation of

111   microtubules that would subsequently polarise cells by serving as oriented

112   conduits in the polarised transport of PCP components [**20**]. Tests of this

113   hypothesis in the adult abdomen have given mixed results [**21-23**]. Results from

114   both wing and the abdomen are conflicting; regions of both appear to be

115   polarised independently of the microtubules [**23**]. In the hope of clarifying this

116   confusing situation we now report our studies of microtubule orientation *in vivo*

117   in the larva. The larva has some advantages over imaginal discs or the adult

118   abdomen: individually identifiable cells have a defined polarity and larval cells

119   are much larger than the adult cells allowing more precision in plotting of the

120   orientation of the microtubules. Several analyses of our own results on the larval

121   abdomen and of raw data kindly provided by Axelrod from the pupal abdomen

122   [**22, 23**] do not support the hypothesis that PCP is oriented by microtubules.

123   In this paper we add to our knowledge of PCP in the larval segment; our

124   two most important findings are to define cell polarity in all the cells of the entire

125   segment and to provide data arguing strongly that orientation of the

126   microtubules does not correlate with the axis of denticle polarity.

MATERIALS AND METHODS

Mutations and Transgenes

Flies were reared at 25°C on standard food. The FlyBase [**24**] entries for the mutant alleles and transgenes used in this work are the following: *ds*: *ds^{UA071}*; *en.Gal4*: *Scer\GAL4^{en-e16E}*; *sr.Gal4*: *sr^{md710}*; *UAS.act::GFP*: *Dmel\Act5C^{UAS.GFP}*; *UAS.DsRed*: *Disc\RFP^{UAS.cKa}*; *UAS.EB1::EGFP*: Eb1^{UAS.GFP}; *UAS.ectoDs*: *ds^{ecto.UAS}*; *UAS.LifeAct::mCherry*: *Scer\ABP140^{UAS.mCherry}*; *UAS.RedStinger*: *Disc\RFP^{DsRedT4.UAS.Tag:NLS(tra)}*; *UAS.ovo*: *ovo^{svb.Scer\UAS}*; *act>stop>d::EGFP*: *d^{FRT.Act5C.EGFP}*; *DE-cad::tomato*: *shg^{KI.T:Disc\RFP-tdTomato}*; ds::EGFP: *Avic\GFP^{ds-EGFP}*; *hs.FLP*: *Scer\FLP1^{hs.PS}*; *sqh.UTRN::GFP*: *Hsap\UTRN^{Scer\UAS.P\T.T:Avic\GFP-EGFP}*; *tub>stop>Gal4*: *Scer\GAL4^{FRT.Rnor\Cd2.αTub84B}*.

Experimental Genotypes

(**figure 1A)** *y w hs.FLP/ w; DE-cad::tomato/ en.Gal4 UAS.act::GFP*.

(**figure 1B)** *w; DE-cad::tomato sqh.UTRN::GFP*.

(**figure 2,** and **table 1)** *w; ds^{UA071} DE-cad::tomato sqh.UTRN::GFP/ DE-cad::tomato sqh.UTRN::GFP; sr.Gal4/ UAS.ectoDs*.

(**figures 3, 4)** *w; ds::EGFP FRT40A*.

(**figures 5A,B, 6)** *y w hs.FLP/ w; en.Gal4 UAS.DsRed/ +; act>stop>d::EGFP/ +*.

(**figures 5C,D, S2, 6)** *y w hs.FLP/ w; DE-cad::tomato; act>stop>d::EGFP/ +*.

(**figures 7, S3)** *y w hs.FLP/ w; tub>stop>Gal4/ DE-cad::tomato; UAS.ovo/ UAS.EB1::EGFP*.

(**figures 8, S4, S6,** and **movies 1, 2)** *y w hs.FLP/ w; tub>stop>Gal4/ DE-cad::tomato; UAS.EB1::EGFP/ UAS.LifeAct::mCherry*.

(**figure S1)** *w; ds::EGFP FRT40A/ +; UAS.ectoDs/ sr.Gal4 UAS.RedStinger*.

Live Imaging of Larvae

To induce clones expressing *d::EGFP*, *ovo*, or *EB1::EGFP*, 2-4 h AEL embryos were heat shocked on agar plates with fresh yeast paste at 33°C for 30 min in a water bath. Larvae were grown at 25°C for 47-52 hr and moved to fresh standard food

155 for 2-4 h (tagged Ds, D, and EB1) or 10-15 hr (predenticles) before imaging.

156 Second stage larvae were washed in water and then immobilised between a glass

157 slide and coverslip by exploiting the surface tension of a drop of Voltalef 10S oil

158 or water. Epidermal cells in the A4-A7 abdominal segments of the larvae were

159 imaged live through the cuticle using a Leica SP5 inverted confocal microscope

160 with a 63x/1.4 oil immersion objective. Tagged fluorescent proteins were excited

161 sequentially with 488nm and 561nm laser beams and detected with 510-540nm

162 and 580-630nm emission filters, using Leica HyD hybrid detectors.

Quantification of Ds Amounts at Cellular Interfaces

164 Ds::EGFP membrane distribution was analysed in the apical plane of ventral

165 epidermal cells of early second stage larvae. Two juxtaposed areas of the

166 segment (the denticulate and undenticulate regions) were imaged separately to

167 grant sufficient resolution and subsequently merged, and maximum intensity

168 projections of typically 4μm stacks were used to compensate for ruggedness in

169 the denticulate region. Between 3 and 12 images from different larvae were

170 acquired and aligned to the mediolateral axis using rows of tendon cells as

171 reference. Ten straight lines parallel to the anteroposterior axis and 4μm wide

172 were drawn over the images at random heights, and the profile of average

173 fluorescence intensity along each line was plotted. Each profile displayed peaks

174 where the line intersected cell boundaries: the fluorescence maxima were

175 quantified using the BAR collection of ImageJ routines [**25**] and manually

176 assigned to the respective cellular interfaces. Due to cell morphology and image

177 noise not every line could provide a measure for each interface, therefore for

178 every image a value of mean intensity was calculated only for cell boundaries

179 intersected by at least 3 lines. The mean of means of all boundaries in an image

180 was used as reference to normalise the fluorescence intensity maxima.

Mapping of D polarity

182 D polarity at the plasma membrane was assessed over the whole segment by

183 analysing a total of 594 cells from small clones expressing *d::EGFP* in the ventral

184 epidermis of 44 different larvae. Each cell was assigned a row number and

185 polarity: rows of cells were identifiable by proximity to conspicuous landmarks

186   like denticles, sensory cells, and tendons with unique shape, while polarity was

187   scored by eye based on whether D::EGFP fluorescence was exclusively on the

188   anterior (Anterior membrane) or posterior (Posterior membrane) side of their

189   plasma membrane, unpolarised but clearly enriched at the membrane (Uniform

190   membrane), or homogeneously distributed in the cytoplasm (Uniform

191   cytoplasm).

Analysis of Microtubule Growth Direction

193   Orientation of growing microtubules was analysed following EB1::EGFP comets

194   in ventral larval epidermal cells. Clonal expression of *EB1::EGFP* was necessary

195   to avoid interference from the strong signal of underlying muscle cells, and

196   undenticulate regions were preferred because denticles obscured the fluorescent

197   signal. Early second stage larvae were mounted in a small drop of water ensuring

198   their posterior spiracles were out of the liquid, and movies of individual cells

199   were recorded at 5.16 s intervals for typically 5 min, imaging a single 0.773µm

200   apical confocal plane. Movie frames were registered using the ImageJ plugin

201   Stackreg [26] to account for slight movements of the larvae. Cells were then

202   aligned to the mediolateral axis using the T3 row of tendon cells and rows of

203   denticles as references, and cells situated in the right hemisegments were flipped

204   to match the mediolateral orientation of the left hemisegment cells. Two cells,

205   one in the A compartment (row 7 or 8) and one in the P (row -2 or -1), were

206   selected from each of 10 larvae and pooled for blind analysis. Comets were

207   traced manually using the ImageJ plugin MtrackJ [27], sampling all the visible

208   comets within each cell for as many time points as were necessary to count 150-

209   200 comets per cell, and angles of the comets' trajectories relative to the

210   anteroposterior axis of the larva were derived from the first and last time point

211   of their tracks.

Data Analysis

213   Data analysis was carried out in R 3.5.3 [28], using the *CircMLE* [29], *circular*

214   [30], *DescTools* [31], *dplyr* [32], *ggplot2* [33], and *mosaic* [34] packages.

RESULTS

Comparing wildtype and polarity modified larvae

(i) Background

In this section we reexamine and test the model as exemplified by those single

cells described as "atypical" in which one face of the cell's membrane abuts two

different neighbours [**17**]. Some of these cells are multipolar and these exemplify

very strongly the argument that PCP stems from a comparison between the

facing membranes of a single cell. These atypical and multipolar cells are now

studied in "polarity modified" larvae, in which the overall segmental polarity has

been considerably modified by experiment. Unlike previously, we study the

predenticles, that is denticles observed prior to the deposition of cuticle.

We compare the cell polarity of wildtype [**15, 17**] and polarity modified

larvae (**figure 2**). To make the polarity modified larvae, we engineer increased

expression of an active form of *ds* in T1 and T2 cells (*sr.Gal4 UAS.ectoDs* [**15**]);

this changes the landscape of Ds activity, making peaks (instead of troughs, as in

the wildtype) in T1 and T2. Consequently, the polarities of rows of cells 1, 2, 4

and 5, that abut T1 and T2, now point inwards; that is reversed from the

wildtype (**figure 2**). The other rows, 0, 3 and 6 could also be affected because

polarity can be propagated beyond the neighbouring cells [**8, 9, 15**]. To explain

further how the Ds/Ft machine propagates polarity changes from cell to cell: an

increase in Ds activity in cell *a* attracts more Ft on the facing membrane of cell *b*.

On that facing membrane more Ft tends to exclude Ds activity, enabling more Ds

to accumulate on the far side of cell *b* which will, in turn, draw more Ft to the

facing membrane of cell *c* [**5, 7**].

(ii) Atypical cells

In all larvae, the numbered cell rows are often irregular and some atypical cells may individually abut on the same side two neighbours, each with a different level of Ds activity. We compare the predenticles of atypical cells in wildtype and polarity modified larvae. In the wildtype, one posterior part of cell *a* in row 4 may contact a T2 neighbour with a lower Ds activity than row 3 (the associated predenticles in this region of cell *a* point anteriorly) and a separate part of cell *a* may contact a row 4 neighbour with a higher Ds activity than row 3 [17]. However, in the polarity modified larvae, the predenticles of nearly all cells of row 4 (typical and atypical cells) point posteriorly —this is as expected from the model because *both* types of posterior neighbour that can abut a row 4 cell (T2 and another row 4 cell) now have higher levels of Ds activity than the anterior neighbour, a row 3 cell (**figure 2A-C** and **table 1**). However for these polarity modified larvae, some single atypical cells of row 2 have two anterior neighbours —cells of T1 and row 2— that are higher and lower in Ds activity than the posterior neighbour of the atypical cell, respectively. Consequently, the model predicts that their associated predenticles should point forwards in that part of the cell that abuts T1 and backwards in that part of the same cell abutting row 2, and they do (**figure 2D-F** and **table 1**). There are some quantitative differences between the current data and the wildtypes we scored earlier ([17], see legend to **table 1)**. Nevertheless, these results, especially on the polarity modified larvae, confirm and strengthen a model of PCP in which cells in a tissue are polarised due to an underlying gradient of Ds activity. They are not sufficient to exclude a model in which polarisation depends only on local interactions between cells.

Direct assessment of Ds distribution in both wildtype and polarity modified larvae

We measure the native Ds distribution using a tagged Ds molecule expressed as in the wildtype. Ds accumulates as puncta in the membrane (**figure 3**, [14, 35]) and, presumably, the puncta contain or consist of Ds-Ft heterodimers [36].

We previously inferred but did not show directly a supracellular gradient in Ds activity that rises within the A compartment reaching a peak near the rear of that compartment and then falling into the P [16]. We therefore quantified and

274   compared the amount of Ds localised at cell junctions in all rows of the segment

275   in the larval ventral epidermis. These measurements do not evidence an overall

276   gradient. However, both junctions 9/T3 and T3/10 show a higher amount of

277   tagged Ds than the other boundaries; these junctions are located near the rear of

278   the A compartment (**figure 4**). We applied the same quantitation technique to

279   polarity modified larvae and found that the distribution of Ds is altered from the

280   wildtype as expected (**figure S1**), in a way that validates our quantification

281   technique and consequently the existence of a peak of Ds levels near the rear of

282   the A compartment in the wildtype (**figure 4**).

The location of Dachs

284   The myosin-related molecule D is a marker of polarity and localised by the Ds/Ft

285   system [**5, 14, 37-39**]. It is usually asymmetrically distributed on a polarised cell

286   and is thought to co-localise with the face of the cell associated with the most Ds

287   [**14, 38, 39**]. We map D to the membranes of individual cells in the larval

288   epidermis by making small clones of cells that express tagged D; this allows the

289   distribution of D on a particular cell to be assessed so long as the neighbour(s)

290   does not contain any tagged D.

291   We examine the distribution of D in wildtype larvae in order to reveal the

292   molecular polarity of cells that lack denticles (**figures 5, 6**). In the P

293   compartment, all the denticulate and undenticulate cells show a consistent

294   molecular polarity, D being localised posteriorly in the cell. Most cells of the A

295   compartment have the opposite polarity, with D located anteriorly. In both

296   compartments, the location of D in the denticulate cells correlates in all cases

297   with the denticle polarity, and this includes the cells of rows 0, 1 and 4 whose

298   denticles point forward. The tendon cells, T1, T2 and T3 can express D but it is

299   mostly cytoplasmic in location. The cells flanking T1 and T2 (but not T3)

300   accumulate D at the membrane abutting the tendon cells. Unlike all the other

301   rows, cells of row 11 show some variation in the localisation of D: about 45%

302   localise it at the posterior cell membrane, as do cells in the P compartment; in

303   35% it is at the membrane but not asymmetrically localised and, in the

304   remaining cells, D is either at the anterior or found only in the cytoplasm (**figure

305   6**). This means that the line where polarity changes from the A-mode to the P-

306   mode is not at the A/P border [**16**] but anterior to it; suggesting that the second

307   cell row anterior to the A/P cellular interface (row 10) contains the peak level of

308   Ds activity. From that row, effects on polarity spread forwards into the A

309   compartment and backwards into row 11 and the P compartment (see model in

310   **figure 9**).

311   The localisation of D is not always continuous along the entire face of a cell.

312   When the plasma membrane of one side of an atypical cell **a** abuts two separate

313   cells, and our model implies that these two cells have different levels of Ds

314   activity, then the D from cell **a** is localised at the interface with just one of those

315   cells, on that part of the membrane that has most Ds activity (cells 10 and 11 in

316   **figure 5C**, and **figure S2**, see legend). This suggests that different parts of a

317   single cell's membrane can compete for D.

ovo-expressing clones reveal otherwise unseen polarity.

319   Small clones that overexpress *ovo* in naked areas often produce denticles in

320   embryos [**40, 41**]. We made marked clones in larvae and these also generally

321   made denticles. The denticles showed a consistent orientation, pointing forwards

322   in P and backwards in most of A, exactly mirroring the polarity pattern as

323   identified by D localisation (**figure 7,** compare with **figure 6**). Thus, cells of row

324   11 at the rear of the A compartment mostly made denticles that pointed

325   forwards (**figure 7**) as is characteristic of cells belonging to the P compartment.

326   Just as signalled by the localisation of D, in a minority of row 11 cells, polarity

327   was ambiguous with denticles pointing in various directions (**figure S3**). The

328   denticles belonging to the cell row 10 anterior to row 11 always pointed

329   backwards and denticles of the row behind row 11 (row -2 of the P

330   compartment) always pointed forwards.

Does the orientation of growing microtubules correlate with PCP?

332   We study the orientation of growing microtubules (using EB1 comets, [**42, 43**])

333   in the large epidermal cells of the ventral larva. Our main data is collected from

334   identified A cells of rows 7-8 (direction of PCP is posterior) and identified P cells

335   of rows -2 and -1 (direction of PCP is anterior; **figure 6**); the classification of the

336   A and P cells as having opposite polarities is based on studies of the larval

337   ventral abdomen described above. To assess the orientation of growing

338   microtubules, we took 10 larvae, made films and studied one A and one P cell

339   from each (**movies 1, 2**). The growing microtubules were then recorded vis-à-vis

340   the axis of the larva by one person (SP) who was blinded to the identity of each of

341   the 20 cells he was scoring. The orientations of about 4000 EB1 comets are

342   shown and analysed in **figure 8**.

343   In the wing, the predominant alignment of the microtubules is close to the

344   axis of PCP [**20, 44**]. By contrast, in the larval epidermal cells, in both A and P

345   compartments, the majority of the microtubules are aligned perpendicular to the

346   anteroposterior axis, the axis of PCP (**figure 8A,B**). To analyse our data and

347   following the approach in the wing, the comets of the larvae are sorted into four

348   90 degree quadrants centred on the anteroposterior and mediolateral axes and

349   their frequencies plotted. The quadrants are described as "anterior", "posterior",

350   "medial" and "lateral" (**figure 8C,D**). The axis of PCP lies in the anteroposterior

351   axis, but, in A compartment cells, 66% of the total angles of growth fall within the

352   medial and lateral sectors, while in the P compartment the comparable figure is

353   71%. Clearly there is no overall correlation between microtubular orientation

354   and PCP, belying the hypothesis that microtubular orientation is causal for PCP.

355   However, we could look for a limited correlation between the orientation of

356   growing microtubules and the direction of PCP. For example, considering only

357   the minority of microtubules within the anterior and posterior sectors, we find

358   insignificant differences in polarity (**figure 8C,D**). In A cells the proportion of all

359   microtubules that grow anteriorly is 15.8% with a 95% CI of [13.5 to 18.2] and

360   the proportion that grow posteriorly is 18.3% [15.9 to 20.6]. In P cells it is the

361   reverse; 16.7% grow anteriorly [14.4 to 19.1] and the proportion that grow

362   posteriorly 12.7% [10.3 to 15.0]. There was a comparably weak bias in the

363   medial and lateral quadrants: in A cells a larger proportion of all microtubules

364   grow medially 34.4%[32.0 to 36.8] than laterally 31.5% [29.1 to 33.8] while the

365   reverse bias occurs in P cells where more microtubules grow laterally 36.9%

366   [34.5 to 39.2] than medially 33.7% [31.4 to 36.1] (**figure 8C,D**).

367   How uniform are the individual cells? To answer we group all the growing

368   microtubules according to which cell (and larva) they come from and according

369 to which of four 90 degree quadrants they fall into (**figure 8E**). Remarkably, in

370 all sets, individual cells differ wildly from each other. Comparing the anterior

371 versus posterior and medial versus lateral quadrants we find no strong evidence

372 for a bias in the directions in which the microtubules grow —apart from the

373 obvious and main finding that most of the microtubules grow more or less

374 perpendicular to the axis of PCP.

375 Could there be a special subset of oriented microtubules perhaps aligned

376 close to the anteroposterior axis, the axis of PCP, that might show a polarity bias

377 that related to some function in planar polarity? There is no independent

378 evidence favouring such a perspective. Nevertheless, to check we scan through

379 the entire circumference in 22.5 degree sectors, measuring the amount of bias in

380 the microtubules that fall within opposite pairs of sectors. There is no increase in

381 bias in the sectors that included the axis of PCP in either the A or the P

382 compartments, nor in nearby sectors. However, there is a local peak of bias

383 within the A compartment: there is a significant bias in the number of growing

384 microtubules within one pair of 22.5 degree sectors that is far away from the axis

385 of PCP. Within the P compartment a similar peak of bias is centred near the

386 mediolateral axis within two facing 22.5 degree sectors (**figure S4**). But note that

387 these biases represent only 2-3% of the total population of microtubules. Thus,

388 although we found some irregularities in the circular distribution of growing

389 microtubules, we find no correlation with the axis of PCP.

390 Axelrod's group kindly made their raw data from the pupal abdomen

391 available to us and we treat them exactly as our larval data. Axelrod and

392 colleagues grouped the angles of growing pupal comets into two unequal sets

393 (two broad sectors of 170 degrees, each including the anteroposterior axis, were

394 compared to each other, while the remaining microtubules were grouped into

395 two narrow mediolateral sectors of 10 degrees each [**22, 23**]). But for our

396 analysis, to conform with how data on the wing have been presented [**20, 22,**

397 **23**], and to allow a comparison with our results, we subdivided their data into

398 four 90 degree quadrants. Even more so than in the larva, the majority of the

399 pupal microtubules are oriented orthogonally to the axis of PCP (**figure S5A-D**):

400 69% of the total population of growing microtubules in the A compartment are

401   aligned within the quadrants centred on the mediolateral axis, while in the P

402   compartment the comparable figure is 73% (**figure S5C,D**). This finding does not

403   fit comfortably with a hypothesis that microtubular orientation drives PCP.

404   Further comparison of the Axelrod group's data on the pupa with ours on

405   the larva show some quantitative differences. Unlike ours on the larva, their

406   pupal data show statistically significant biases in the orientation of comets

407   (**figure S5C,D**). In A cells the proportion of all microtubules that grow anteriorly

408   is 12.7% with a 95% CI of [11.3 to 14.1], significantly smaller than the

409   proportion that grow posteriorly 18.1% [16.6 to 19.5]. In P cells we see a reverse

410   bias: 15.8% [13.3 to 18.2] grow anteriorly and 11.5% [9.1 to 13.9] posteriorly.

411   Notably, there is a comparable and also significant bias in the medial and lateral

412   quadrants but in the same direction in both compartments. In A cells a larger

413   proportion of all microtubules grow laterally 38.1% [36.7 to 39.6] than medially

414   31.1% [29.7-32.5] and a similar bias occurs in P cells where 39.8% [37.4-42.3]

415   grow laterally and 32.9% [30.5-35.3] grow medially (**figure S5C,D**).

416   We then plotted all the growing microtubules according to which pupa they

417   came from and according to which of four 90 degree sectors they fell into (**figure**

418   **S5E**). Individual pupae differ wildly from each other. In both our results on the

419   larva and Axelrod's results in the pupa, there is considerable inconsistency

420   between individuals (compare **figure 8E** with **figure S5E**). Only when all cells

421   are taken together is there any overall and significant polarity bias in Axelrod's

422   data.

423   We classified the growing microtubules in Axelrod's data into 22.5 degree

424   sectors and looked for an orientation bias within opposite pairs of sectors. We

425   find examples of significant bias shown by the microtubules in various sector

426   pairs and these are mostly not near the axis of PCP. In A cells there is a

427   statistically significant and local peak of bias ca 60-80 degrees divergent from the

428   axis of PCP. In P cells there is a statistically significant and local peak of bias ca

429   35-55 degrees divergent from the axis of PCP (**figure S4**). These observations do

430   not fit with the conjecture that a special set of oriented microtubules, in or close

431   to the PCP axis, might be driving planar polarity.

432   Dividing the data into sectors gives the impression of biases in the

433 anteroposterior as well as in the mediolateral axes (although these are non

434 significant in the case of the larva). But, because we suspect that subdividing the

435 angles into sectors may lead to erroneous conclusions we investigated the

436 distributions of the angles as a whole. We took the angular data of the A and P

437 cells of the larva and pupal abdomen and using a maximum likelihood model

438 approach [**29**], we found that the best fit in all four cases is to a distribution with

439 two peaks each roughly 90 degrees divergent from the axis of PCP (**figure S6**).

440 Unexpectedly, there are slight deviations of these peaks in the bimodal

441 distributions; in all four distributions one of the peaks deviates 10 degrees from

442 the mediolateral axis. Interestingly, the direction of deviation is opposite in the A

443 cells to that in the P cells; in both sets of A cells one of the peaks is tilted 10

444 degree towards the posterior hemi-circumference, whereas in both sets of P cells

445 one of the peaks is tilted 10 degrees towards the anterior hemicircumference

446 (**figure S6**, see legend). These opposite deviations in A and P cells may be the

447 basis of the apparent but weak biases we observe when dividing the data into

448 four quadrants.

DISCUSSION

450 ### A gradient model?

451 In trying to understand planar cell polarity, *Drosophila* has proved the most

452 amenable and useful experimental system. Using the *Drosophila* larva, we have

453 built a model of how the Ds/Ft system determines the pattern of polarity in the

454 abdominal segment [**16, 17**]. In this model the Ds/Ft system converts graded

455 slopes in the expression levels of *ds* and *fj* into local intercellular differences in

456 the levels of Ds activity, and into PCP without any intervention by the Stan/Fz

457 system [**5**].

458   Here we have reexamined the model and extended it to those uncharted

459 parts of the larval segment that lack denticles (**figure 9**). All the observations we

460 have made give results that are consistent with and support the model. However

461 it is not clear whether the model requires interactions between Ds, Ft and Fj to

produce a multicellular gradient of Ds levels at the cell membranes, and expectations on this differ [36]. We originally proposed that the levels of Ds activity would be graded in opposite ways in the A and the P compartment and ultimately these gradients would be read out as PCP in each of the cells [16]. We imagined that multicellular gradients of Ds activity would persist and span the whole field of cells and this has been assumed by most [5, 7, 45, 46] and actually detected, locally, in the migrating larval epidermal cells in the pupa [47]. Alternatively, once the arrow of polarity has been established in each cell, a feedback mechanism could result in a redistribution of bridges so that, ultimately, each cell would contain the same numbers of bridges, similarly disposed— there would be no persistent multicellular gradient in Ds activity (eg [36]). However there would still be differences in the dispositions and orientations of Ds-Ft bridges between the opposite membranes of each cell. Our current measurements of Ds levels do not settle the matter: we did not detect a pervasive gradient of Ds, but amounts were not flat either. We found a peak in Ds level located near the rear of the A compartment near where a Ds activity gradient was predicted to summit. However a shallow Ds gradient could still exist — it might be missed because we quantify only the total Ds present in abutting pairs of membranes. This shortcoming means that the results can neither tell us the cellular provenance of the Ds we measure, nor reveal how much of it is in Ds-Ft or in Ft-Ds bridges within the apposed membranes. Thus, if any cell has a higher level of Ds, this Ds will bind more Ft in the abutting cell membrane, and, we believe, tend to exclude Ds from that abutting membrane. These effects will tend to even out the amounts of Ds in joint membranes and therefore tend to disguise any gradients, local peaks or troughs.

Could one build the segmental pattern of polarity using only a peak plus propagation, thereby managing without any initial gradient of *ds* expression? If so, a localised peak in amount of Ds at the rear of the A compartment (with a maximum in row 10) could affect polarity forwards into row 9 and beyond, and propagate backwards through row 11 into the P compartment. The single cell troughs in Ds activity in T1 and T2 would orient the polarity of the flanking cells to point away from these tendon cells. All these polarity effects would reinforce each other to make a more robust pattern. However, if there were no initial

495 gradient of *ds* expression, only row 3 would present a problem; in order to

496 explain why it points backwards, the trough of T1 in Ds activity would need to be

497 deeper than that of T2 (see figure 4 in [**15**]). Perhaps it will prove important to

498 note that the gradient model and the alternative localised peak and troughs

499 model just outlined are not mutually exclusive and each can contain aspects of

500 the truth.

501   Originally predicted to be at the A/P compartment border [**16**] we

502 conclude now that a Ds peak occurs two cells anterior to that border, in row 10

503 (**figure 9**, a similar peak two cells from the A/P border has been described in the

504 dorsal abdomen of the pupa [**47**]). This observation is supported by both D

505 localisation and the orientation of ectopic denticles formed by *ovo*-expressing

506 clones. There are interesting implications: the peak in Ds protein at the cell

507 junctions is in a cell that is flanked on both sides by A compartment cells, the

508 most posterior of which (row 11) has "P type" polarity. Why is this summit out of

509 register with the lineage compartments? It could be that this peak is specified by

510 a signal emanating from one compartment and crossing over to affect the next

511 compartment. There are precedents for this kind of transgression [**48-52**]. Also,

512 in the abdomen of the developing adult fly, Hedgehog signal spreads from the P

513 compartment across into the A compartment and induces different types of

514 cuticle at different distances [**53**].

515   Our results can best be interpreted, as others have done [**14, 37, 54**], that D

516 acts as an eloquent marker of a cell's polarity, is localised on the membrane with

517 the most Ds, and acts immediately downstream of the Ds/Ft system.

Microtubules and PCP

519 We have suggested [**17**] that intracellular conduits might be involved in a local

520 comparison between facing membranes of a cell and shown here that this

521 perspective successfully predicts which cells should become bipolar even in

522 polarity modified larvae. But there is still no direct evidence for the conduits, and

523 no knowledge of, if they do exist, what they are. One could imagine a set of

524 microtubules, initiated on the membrane, that could align more or less with the

525 anteroposterior axis and traverse the cell to meet the membrane opposite.

526 Indeed, Uemura's group have proposed that microtubules, oriented by the Ds/Ft

527   system, translocate vesicles carrying PCP components such as Frizzled (Fz) and

528   Dishevelled (Dsh) to one side of a cell to polarise it. Their hypothesis began with

529   observations on microtubule-dependent transport of tagged proteins *in vivo* in

530   cells of the wing disc [**19**] and was extended by the use of EB1 comets to plot

531   microtubule polarity in the pupal wing [**20-23**]. Harumoto and colleagues

532   studied the proximal part of the wing where they found a transient correlation,

533   with a small majority of the microtubules growing distally, but there was no such

534   correlation in the distal wing. Also, in *ds⁻* wings, distal regions show consistently

535   polarised microtubules (a small majority now grow proximally), although the

536   hairs in that region still point distally [**20**]. Likewise, while some studies of the

537   adult abdomen demonstrate a local correlation between cell polarity and the

538   orientation of limited subsets of microtubules, PCP in other parts did not show

539   this correlation and the authors concluded that, in those parts, polarity is

540   determined independently of the microtubules [**23**]. We have tested the

541   hypothesis that microtubular orientation drives PCP in the larval abdomen of

542   *Drosophila* and there it also meets serious difficulties. The greatest of these is

543   that most of the microtubules are aligned orthogonally to the axis of PCP (this

544   fact is also extractable from the pupal data kindly provided by Axelrod's group).

545   Of the roughly 30% of all microtubules that fall into the two quadrants centred

546   on the axis of PCP, there is a small net excess, corresponding to about 5% of the

547   total, that could perhaps result in a net transport of vesicles in the direction of

548   PCP. But even if this were so, more than 80% of the vesicles carrying cargo

549   should arrive in the wrong part of the cell membrane.

550   Why are there apparent biases in microtubule orientation in the data? An

551   analysis of the circular distribution of comets showed, in all the sets of data (ours

552   and those of Axelrod's group), a deviation of 10 degrees in one of the peaks of the

553   bimodal distribution of the angles (**figure S6**). This deviation, plus the precise

554   orientation of the 90 degree quadrants, may explain the apparent bias of

555   microtubular orientation seen clearly in the Axelrod data and hinted at much

556   more weakly in our data. How? Imagine a circular bimodal distribution

557   composed of two separate unimodal distributions: the tails of both probability

558   distributions would be closer and overlap more if the distance between the mean

559   angles were reduced. In our cases, one of the tails of the distributions whose

560   mean angles deviate by 10 degrees will decrease slightly the frequency of angles

561   within one of the anteroposterior quadrants and concomitantly the other tail

562   increase the frequency in the opposite anteroposterior quadrant. This deviation

563   may have its origin in a correlation between cell shape and microtubular

564   orientation [**44, 55, 56**] and in different cell shapes in the A and P cells; these are

565   more obvious at or close to the A/P border [**57**].

566   The hypothesis of Uemura's group which proposes that microtubules

567   transport Fz to one side of the cell to polarise it meets an additional problem in

568   the larval abdomen. The normal orientations of the denticles in the larva does

569   not require input from the Stan/Fz system; indeed the Ds/Ft system appears to

570   act alone [**7-9**]. But could oriented microtubules be involved in PCP, even

571   without any role of the Stan/Fz system? Our results from the larval abdomen say

572   no. We cannot exclude the possibility of a small subset of stable microtubules

573   (undetectable because they would not bind EB1), aligned with the

574   anteroposterior axis and strongly biased in polarity, in the pupal or larval

575   abdomens (or proximodistal axis in the wing). There is no evidence for such

576   microtubules, but if they exist their number and bias in orientation must be

577   strong enough to overcome the moving of vesicles on the unbiased dynamic

578   microtubules we have studied.

Conclusions

580   We have enhanced our present model of how the Ds/Ft system generates the

581   intricate polarity of the larval segment. The key element of this model is that

582   each cell compares its neighbours and is polarised (and points its denticles)

583   towards the cell presenting the most Ds activity. This hypothesis gains more

584   support from our new results on the multipolarity of single cells. But we have not

585   found out how the comparison is made: an attractive hypothesis by others was

586   that oriented microtubules are the critical agent, but, if we interrogate our data

587   for biases in polarity within all the growing microtubules, or if we select subsets

588   of microtubules whose orientations are related to the axis of PCP, we do not find

589   evidence for a link between microtubular polarity and the polarity of the

590   denticles (the "direction" of PCP). Using two different methods we demonstrated

591   that undeticulated cells are also polarised and their polarity is as the model

592 predicts, and that the point where the amount of Ds is, presumably, highest and

593 from where, like a watershed divide, polarity diverges, is two cells away from the

594 compartment border. We looked to demonstrate the predicted multicellular

595 gradient of Ds but, possibly because of an insufficiency in our methods, we only

596 found a localised peak (at the rear of the A compartment as the model requires).

597 Thus, if there is a multicellular gradient of Ds activity, it must be very shallow.

598 There's still much to do; still so much to learn.

ACKNOWLEDGEMENTS

COMPETING INTERESTS

604 The authors declare that no competing interests exist.

FUNDING

REFERENCES

608 1   Goodrich, L. V., Strutt, D. 2011 Principles of planar polarity in animal
609   development. *Development.* **138**, 1877-1892. (10.1242/dev.054080)

610 2   Henderson, D. J., Long, D. A., Dean, C. H. 2018 Planar cell polarity in organ
611   formation. *Curr. Opin. Cell Biol.* **55**, 96-103. (10.1016/j.ceb.2018.06.011)

612 3   Devenport, D. 2016 Tissue morphodynamics: Translating planar polarity
613   cues into polarized cell behaviors. *Semin. Cell Dev. Biol.* **55**, 99-110.
614   (10.1016/j.semcdb.2016.03.012)

615 4   Butler, M. T., Wallingford, J. B. 2017 Planar cell polarity in development and
616   disease. *Nat. Rev. Mol. Cell Biol.* **18**, 375-388. (10.1038/nrm.2017.11)

5   Lawrence, P. A., Casal, J. 2018 Planar cell polarity: two genetic systems use one mechanism to read gradients. *Development.* **145**, (10.1242/dev.168229)

6   Carvajal-Gonzalez, J. M., Mlodzik, M. 2014 Mechanisms of planar cell polarity establishment in Drosophila. *F1000Prime Rep.* **6**, 98. (10.12703/P6-98)

7   Casal, J., Lawrence, P. A., Struhl, G. 2006 Two separate molecular systems, Dachsous/Fat and Starry night/Frizzled, act independently to confer planar cell polarity. *Development.* **133**, 4561-4572. (10.1242/dev.02641)

8   Donoughe, S., DiNardo, S. 2011 dachsous and frizzled contribute separately to planar polarity in the Drosophila ventral epidermis. *Development.* **138**, 2751-2759. (10.1242/dev.063024)

9   Repiso, A., Saavedra, P., Casal, J., Lawrence, P. A. 2010 Planar cell polarity: the orientation of larval denticles in Drosophila appears to depend on gradients of Dachsous and Fat. *Development.* **137**, 3411-3415. (10.1242/dev.047126)

10 Simon, M. A., Xu, A., Ishikawa, H. O., Irvine, K. D. 2010 Modulation of Fat:dDchsous binding by the cadherin domain kinase Four-jointed. *Curr. Biol.* **20**, 811-817. (10.1016/j.cub.2010.04.016)

11 Ishikawa, H. O., Takeuchi, H., Haltiwanger, R. S., Irvine, K. D. 2008 Four-jointed is a Golgi kinase that phosphorylates a subset of cadherin domains. *Science.* **321**, 401-404. (10.1126/science.1158159)

12 Brittle, A., Repiso, A., Casal, J., Lawrence, P. A., Strutt, D. 2010 Four-jointed modulates growth and planar polarity by reducing the affinity of Dachsous for Fat. *Curr. Biol.* **20**, 803-810. (10.1016/j.cub.2010.03.056)

13 Ambegaonkar, A. A., Pan, G., Mani, M., Feng, Y., Irvine, K. D. 2012 Propagation of Dachsous-Fat planar cell polarity. *Curr. Biol.* **22**, 1302-1308. (10.1016/j.cub.2012.05.049)

14 Brittle, A., Thomas, C., Strutt, D. 2012 Planar polarity specification through asymmetric subcellular localization of Fat and Dachsous. *Curr. Biol.* **22**, 907-914. (10.1016/j.cub.2012.03.053)

15 Saavedra, P., Brittle, A., Palacios, I. M., Strutt, D., Casal, J., Lawrence, P. A. 2016 Planar cell polarity: the Dachsous/Fat system contributes differently to the embryonic and larval stages of Drosophila. *Biol. Open.* **5**, 397-408. (10.1242/bio.017152)

16 Casal, J., Struhl, G., Lawrence, P. A. 2002 Developmental compartments and planar polarity in Drosophila. *Curr. Biol.* **12**, 1189-1198. (10.1016/s0960-9822(02)00974-0)

17 Rovira, M., Saavedra, P., Casal, J., Lawrence, P. A. 2015 Regions within a single epidermal cell of Drosophila can be planar polarised independently. *eLife.* **4**, e06303. (10.7554/eLife.06303)

18 Saavedra, P., Vincent, J. P., Palacios, I. M., Lawrence, P. A., Casal, J. 2014 Plasticity of both planar cell polarity and cell identity during the development of Drosophila. *eLife.* **3**, e01569. (10.7554/eLife.01569)

661   19   Shimada, Y., Yonemura, S., Ohkura, H., Strutt, D., Uemura, T. 2006 Polarized
662   transport of Frizzled along the planar microtubule arrays in Drosophila
663   wing epithelium. *Dev. Cell*. **10**, 209-222. (10.1016/j.devcel.2005.11.016)

664   20   Harumoto, T., Ito, M., Shimada, Y., Kobayashi, T. J., Ueda, H. R., Lu, B.,
665   Uemura, T. 2010 Atypical cadherins Dachsous and Fat control dynamics of
666   noncentrosomal microtubules in planar cell polarity. *Dev. Cell*. **19**, 389-401.
667   (10.1016/j.devcel.2010.08.004)

668   21   Matis, M., Russler-Germain, D. A., Hu, Q., Tomlin, C. J., Axelrod, J. D. 2014
669   Microtubules provide directional information for core PCP function. *eLife*.
670   **3**, e02893. (10.7554/eLife.02893)

671   22   Olofsson, J., Sharp, K. A., Matis, M., Cho, B., Axelrod, J. D. 2014 Prickle/spiny-
672   legs isoforms control the polarity of the apical microtubule network in
673   planar cell polarity. *Development*. **141**, 2866-2874. (10.1242/dev.105932)

674   23   Sharp, K. A., Axelrod, J. D. 2016 Prickle isoforms control the direction of
675   tissue polarity by microtubule independent and dependent mechanisms.
676   *Biol. Open*. **5**, 229-236. (10.1242/bio.016162)

677   24   Thurmond, J., Goodman, J., Strelets, V., Attrill, H., Gramates, L., Marygold, S.,
678   Matthews, B., Millburn, G., Antonazzo, G., Trovisco, V*., et al.* 2019 FlyBase
679   2.0: the next generation. *Nucleic Acids Res.* **47**, D759–D765.
680   (10.1093/nar/gky1003)

681   25   Ferreira, T., Hiner, M., Rueden, C., Miura, K., Eglinger, J., Chef, B. BAR 1.5.1.
682   2017 Available from: https://doi.org/10.5281/zenodo.495245

683   26   Thevenaz, P., Ruttimann, U. E., Unser, M. 1998 A pyramid approach to
684   subpixel registration based on intensity. *IEEE T. Image Process.* **7**, 27-41.
685   (10.1109/83.650848)

686   27   Meijering, E., Dzyubachyk, O., Smal, I. 2012 Methods for cell and particle
687   tracking. *Methods Enzymol.* **504**, 183-200. (10.1016/b978-0-12-391857-
688   4.00009-4)

689   28   R Core Team. R: A Language and Environment for Statistical Computing.
690   Vienna, Austria: R Foundation for Statistical Computing 2019.

691   29   Fitak, R. R., Johnsen, S. 2017 Bringing the analysis of animal orientation
692   data full circle: model-based approaches with maximum likelihood. *J. Exp.*
693   *Biol.* **220**, 3878-3882. (10.1242/jeb.167056)

694   30   Agostinelli, C., Lund. R package 'circular': Circular Statistics (version 0.4-
695   93). 2017 Available from: https://r-forge.r-project.org/projects/circular/

696   31   Signorell, A., multitple authors. DescTools: Tools for Descriptive Statistics.
697   2019 Available from: https://cran.r-project.org/package=DescTools

698   32   Wickham, H., François, R., Henry, L., Müller, K. dplyr: A Grammar of Data
699   Manipulation. 2019 Available from: https://CRAN.R-
700   project.org/package=dplyr

701   33   Wickham, H. 2016 *ggplot2: Elegant Graphics for Data Analysis.* Springer-
702   Verlag New York.

703 34 Pruim, R., Kaplan, D. T., Horton, N. J. 2017 The mosaic Package: Helping
704   Students to 'Think with Data' Using R. *R J.* **9**, 77-102.

705 35 Ma, D., Yang, C. H., McNeill, H., Simon, M. A., Axelrod, J. D. 2003 Fidelity in
706   planar cell polarity signalling. *Nature.* **421**, 543-547.
707   (10.1038/nature01366)

708 36 Hale, R., Brittle, A. L., Fisher, K. H., Monk, N. A., Strutt, D. 2015 Cellular
709   interpretation of the long-range gradient of Four-jointed activity in the
710   Drosophila wing. *eLife.* **4**, e05789. (10.7554/eLife.05789)

711 37 Bosveld, F., Bonnet, I., Guirao, B., Tlili, S., Wang, Z., Petitalot, A., Marchand,
712   R., Bardet, P. L., Marcq, P., Graner, F.*, et al.* 2012 Mechanical control of
713   morphogenesis by Fat/Dachsous/Four-jointed planar cell polarity
714   pathway. *Science.* **336**, 724-727. (10.1126/science.1221071)

715 38 Mao, Y., Rauskolb, C., Cho, E., Hu, W. L., Hayter, H., Minihan, G., Katz, F. N.,
716   Irvine, K. D. 2006 Dachs: an unconventional myosin that functions
717   downstream of Fat to regulate growth, affinity and gene expression in
718   Drosophila. *Development.* **133**, 2539-2551. (10.1242/dev.02427)

719 39 Rogulja, D., Rauskolb, C., Irvine, K. D. 2008 Morphogen control of wing
720   growth through the Fat signaling pathway. *Dev. Cell.* **15**, 309-321.
721   (10.1016/j.devcel.2008.06.003)

722 40 Delon, I., Chanut-Delalande, H., Payre, F. 2003 The Ovo/Shavenbaby
723   transcription factor specifies actin remodelling during epidermal
724   differentiation in Drosophila. *Mech. Dev.* **120**, 747-758. (10.1016/s0925-
725   4773(03)00081-9)

726 41 Walters, J. W., Dilks, S. A., DiNardo, S. 2006 Planar polarization of the
727   denticle field in the Drosophila embryo: roles for Myosin II (zipper) and
728   fringe. *Dev. Biol.* **297**, 323-339. (10.1016/j.ydbio.2006.04.454)

729 42 Akhmanova, A., Steinmetz, M. O. 2008 Tracking the ends: a dynamic protein
730   network controls the fate of microtubule tips. *Nat. Rev. Mol. Cell Biol.* **9**, 309-
731   322. (10.1038/nrm2369)

732 43 Schuyler, S. C., Pellman, D. 2001 Microtubule "plus-end-tracking proteins":
733   The end is just the beginning. *Cell.* **105**, 421-424. (10.1016/s0092-
734   8674(01)00364-6)

735 44 Gomez, J. M., Chumakova, L., Bulgakova, N. A., Brown, N. H. 2016
736   Microtubule organization is determined by the shape of epithelial cells. *Nat.*
737   *Commun.* **7**, 13172. (10.1038/ncomms13172)

738 45 Fulford, A. D., McNeill, H. 2019 Fat/Dachsous family cadherins in cell and
739   tissue organisation. *Curr. Opin. Cell Biol.* **62**, 96-103.
740   (10.1016/j.ceb.2019.10.006)

741 46 Matis, M., Axelrod, J. D. 2013 Regulation of PCP by the Fat signaling
742   pathway. *Genes Dev.* **27**, 2207-2220. (10.1101/gad.228098.113)

743 47 Arata, M., Sugimura, K., Uemura, T. 2017 Difference in Dachsous levels
744   between migrating cells coordinates the direction of collective cell
745   migration. *Dev. Cell.* **42**, 479-497 e410. (10.1016/j.devcel.2017.08.001)

48   Basler, K., Struhl, G. 1994 Compartment boundaries and the control of Drosophila limb pattern by Hedgehog protein. *Nature*. **368**, 208-214. (10.1038/368208a0)

49   Diaz-Benjumea, F. J., Cohen, S. M. 1995 Serrate signals through Notch to establish a Wingless-dependent organizer at the dorsal/ventral compartment boundary of the Drosophila wing. *Development*. **121**, 4215-4225.

50   Doherty, D., Feger, G., Younger-Shepherd, S., Jan, L. Y., Jan, Y. N. 1996 Delta is a ventral to dorsal signal complementary to Serrate, another Notch ligand, in Drosophila wing formation. *Genes Dev.* **10**, 421-434. (10.1101/gad.10.4.421)

51   Lawrence, P. A., Struhl, G. 1996 Morphogens, compartments, and pattern: lessons from Drosophila? *Cell*. **85**, 951-961. (10.1016/s0092-8674(00)81297-0)

52   Tabata, T., Takei, Y. 2004 Morphogens, their identification and regulation. *Development*. **131**, 703-712. (10.1242/dev.01043)

53   Struhl, G., Barbash, D. A., Lawrence, P. A. 1997 Hedgehog organises the pattern and polarity of epidermal cells in the Drosophila abdomen. *Development*. **124**, 2143-2154.

54   Ambegaonkar, A. A., Irvine, K. D. 2015 Coordination of planar cell polarity pathways through Spiny-legs. *eLife*. **4**, e09946. (10.7554/eLife.09946)

55   Picone, R., Ren, X., Ivanovitch, K. D., Clarke, J. D., McKendry, R. A., Baum, B. 2010 A polarised population of dynamic microtubules mediates homeostatic length control in animal cells. *PLoS Biology*. **8**, e1000542. (10.1371/journal.pbio.1000542)

56   Singh, A., Saha, T., Begemann, I., Ricker, A., Nusse, H., Thorn-Seshold, O., Klingauf, J., Galic, M., Matis, M. 2018 Polarized microtubule dynamics directs cell mechanics and coordinates forces during epithelial morphogenesis. *Nat. Cell Biol.* **20**, 1126-1133. (10.1038/s41556-018-0193-1)

57   Umetsu, D., Aigouy, B., Aliee, M., Sui, L., Eaton, S., Julicher, F., Dahmann, C. 2014 Local increases in mechanical tension shape compartment boundaries by biasing cell intercalations. *Curr. Biol.* **24**, 1798-1805. (10.1016/j.cub.2014.06.052)

58   Blair, S. S. 1995 Compartments and appendage development in Drosophila. *BioEssays*. **17**, 299-309. (10.1002/bies.950170406)

59   Sison, C. P., Glaz, J. 1995 Simultaneous confidence intervals and sample size determination for multinomial proportions. *J. Am. Stat. Assoc.* **90**, 366-369. (10.1080/01621459.1995.10476521)

FIGURE LEGENDS

Figure 1. Larval ventral abdomen and Ds activity landscape. (**A**) Overview of a complete segment with cells expressing GFP under the control of the *engrailed* promoter, a marker of the P compartment [**51, 58**]. Note that rows 7-11 and rows -2 and -1 indicate undenticulated rows of cells; before this paper the polarities of these cells were unknown, see later. GFP labels four rows of cells, between the most posterior row of the A compartment (identified by sensory cells, S) and the most anterior row of the following segment (tendon cells T1, see [**18**]). This driver occasionally also weakly labels a few cells at the rear of the A compartment (asterisks), but we have found that these cells do not express other P markers such as *hedgehog* (data not shown). Cell outlines and denticles are labelled in magenta (DE-cad::tomato). Arrows point to sensory cells (s) that we used as positional markers. (**B**) Ventral denticulate area of a mid second stage larva. Predenticles (rows 0 to 6) and tendon cells (rows T1 and T2) are marked in green (UTRN::GFP, labelling actin), and cell boundaries in magenta (DE-cad::tomato). The rows are not completely regular; here, one T2 cell contacts two row 6 cells at the posterior (asterisk) — typically, T2 only contacts row 5 cells. (**C**) A partially documented model of the landscape of Ds and Fj and therefore of PCP in the wild type [**15, 17**]. In this model, a presumed low level of *ds* expression together with a documented high level of Fj reduces Ds activity in T1 and T2. The sloped line in each cell indicates different amounts of Ds activity at its anterior and posterior limits, the direction of the slope correlating with the cell's polarity. Denticle polarity is shown below and is a readout of the presumed landscape of Ds activity: each cell points its denticles towards the neighbour with the higher Ds activity. Two rows of the P compartment are highlighted in blue, tendon cells are shaded in grey. Anterior is to the left in all figures. Scale bars: 20μm.

Figure 2. PCP and atypical cells in polarity modified larvae. Denticulate areas of polarity modified larvae: (**A-C**) an atypical cell in row 4 (having two posterior neighbours with different Ds activity), and (**D-F**) an atypical cell in row 2 (having two anterior neighbours with different Ds activity). Predenticles and denticles in

rows 1, 2 and 4, 5 with polarity opposite from wildtype are highlighted in magenta. (**A,D**) Images of predenticles, tendon cells, and cell boundaries labelled as in **figure 1B**. (**B,E**) Schemes of cell outlines and predenticle orientation. (**C,F**) Models of polarity modified larvae, Ds activity landscape and denticle polarity in cross sections taken at the dotted blue lines in **B,E**. Blue shading indicates P compartment cells, grey denotes tendon cells, magenta marks the atypical cell. Note that, contrary to wildtype [**17**], in polarity modified larvae row 4 atypical cells are monopolar (**A,B**), while row 2 atypical cells are multipolar (**D,E**). For quantitation of predenticle polarity in row 4 and row 2 atypical cells of wild type and polarity modified larvae, see **Table 1**. Scale bars: 20μm.

Figure 3. Ds localisation in the larval ventral abdomen. Larvae expressing *ds*::EGFP from the tagged endogenous *ds* locus [**14**] show a ubiquitous punctate pattern of fluorescence that concentrates on plasma membranes. (**A**) Denticulate and (**B**) undenticulate areas of early second stage larvae; the cell rows exhibit no obvious differences in *ds* expression or distribution, with the exception of the strong signal around T3 tendon cells. (**C**) Detail of Ds localisation in puncta at the cell membrane. 0 to 6, denticle cell rows. 7 to -2, undenticulate cell rows. S, sensory cell. T1, T2, T3, tendon cell rows. Scale bars: 20μm (**A,B**), 10μm (**C**).

Figure 4. Quantitation of Ds levels at cellular interfaces across the segment. (**Top**) Dot plot of normalised fluorescence intensity maxima corresponding to amounts of Ds at boundaries between cell rows of the larval ventral abdomen. Data are pooled from 12 (denticulate area) and 5 (undenticulate area) images of different larvae. Mean value and 95% confidence interval for each interface are indicated in red. Letters arise from Tukey's multiple comparison test between all interfaces; in the Tukey's test, comparisons between pairs belonging to a group with the same letter show a p value equal to or greater than 0.05. Groups can be assigned more than one letter, reflecting "overlap" between different groups. The graph shows no evidence for a segment-wide gradient of Ds accumulation at the cell membranes, however the 9/T3 and T3/10 boundaries are significantly different from all others, indicating a clear peak anterior to the A/P boundary. (**Middle**) Diagram of denticle polarity, as in **figure 1C**. Sensory cells identify

848   rows 8 and 11. (**Bottom**) Comparisons between Ds amounts at posterior and

849   anterior interfaces of each cell row. Differences in mean normalised fluorescence

850   at the opposite sides of a cell are calculated with 95% confidence interval by

851   Tukey's test. Red indicates a significant difference. Note the significant and

852   opposite differences in cell rows 9 and 10, highlighting the presence of a

853   fluorescence peak around T3.

854   **Figure 5.** D polarity at the plasma membrane in small clones. (**A**) Several cells of

855   the A compartment expressing *d::EGFP*: in row 4, where denticles point

856   anteriorly, D is mostly on the posterior membrane; in rows 5, 6 and 7, with

857   posterior-pointing polarity, D accumulates instead at the anterior face of the

858   cells. Round or comma-like structures are due to autofluorescence from

859   overlying denticles. (**B**) A posterior cell (row -2) accumulates D at its rear,

860   arguing for anterior-pointing polarity. P compartment is labelled in magenta by

861   *en.Gal4 UAS.DsRed*. (**C**) Cells of rows 10 and 11, where D localises on the anterior

862   and posterior sides of the plasma membrane, respectively (see **figure S2** for cell

863   outlines). (**D**) Row 10 cell with more D on the anterior side of the cell membrane,

864   suggesting its polarity points backwards. The sensory cell process associated

865   with row 11 also expresses *d::EGFP*, and as with other cells from row 11 has

866   most D at the posterior side. S, sensory cell. Scale bars: 10μm.

867   **Figure 6.** The localisation of D cell by cell. D localisation in all the cell rows,

868   derived from the analysis of small clones expressing *d::EGFP*. Cells where D

869   accumulates on just the anterior side of the plasma membrane contribute to red

870   circles (Anterior membrane), cells where D is only on the posterior side to blue

871   circles (Posterior membrane), cells where D is enriched at the plasma membrane

872   but in an unpolarised manner to grey circles (Uniform membrane), and cells

873   where D is homogeneously distributed in the cytoplasm to orange circles

874   (Uniform cytoplasm). The position of each circle denotes the cell row and

875   percentage of cells with the indicated D localisation in that row; circle area is

876   proportional to the number of cells represented. Since D is thought to

877   accumulate on the side of a cell facing the neighbour with the least Ds, the

878   pattern of D polarity in the undenticulate region suggests that there is a peak of

879 Ds activity in row 10 (see **figure 9** for full model). n = 594 cells from a total of 44

880 larvae.

881 **Figure 7.** *ovo*-overexpressing clones in normally undenticulate areas of the

882 epidermis. (**A**) Clone in the A compartment (cell rows 7, 8, and 9), marked with

883 EGFP and producing ectopic denticles that point backwards. (**B**) Clone in the P

884 compartment (cell row -1), ectopic denticles pointing forwards. Note that

885 denticles are produced somewhat sporadically and that denticle numbers vary

886 per cell. Scale bars: 10μm.

887 **Figure 8.** Analysis of microtubule polarity in larval epidermal cells. (**A,B**) Rose

888 diagrams showing the distribution of growing microtubule direction in cells of

889 the (**A**) anterior and (**B**) posterior compartment. EB1 comets are grouped in bins

890 of 4 degrees, the length of each bin indicating the percentage of comets with a

891 specific orientation. Comets pointing to the left (135-225°, orange quadrant)

892 grow anteriorly, comets pointing to the right (315-45°, pink) posteriorly, up (45-

893 135°, blue) are medial, and down (225-315°, green) are lateral; n is the total

894 number of comets tracked, from the number of cells/larvae indicated in

895 parenthesis. (**C,D**) Frequency of microtubules with either anterior, posterior,

896 medial or lateral orientation in (**C**) A cells and (**D**) P cells. Comets are sorted into

897 four sectors of 90 degrees centred on the anteroposterior and mediolateral axes.

898 The 95% confidence interval for all comets in each quadrant is calculated

899 according to Sison and Glaz [**59**]. (**E**) Dot plot comparing the orientation of

900 microtubules within each cell of the A and P compartment. For every cell, the

901 fraction of comets falling into the anterior quadrant is plotted next to the fraction

902 in the posterior quadrant, medial next to lateral. Lines connecting the twin values

903 from the same cell emphasise the high variability between individuals. Mean

904 percentage and 95% confidence interval of the mean for each set of cells are

905 shown. Overlying numbers display the exiguous difference between means (md)

906 of the anterior versus posterior and medial versus lateral quadrants, with 95%

907 confidence interval estimated by recalculating the difference of the means after

908 resampling the data 10,000 times and finding the 0.025 and 0.975 quantiles of

909 the resulting distribution of values; P-values were obtained as the frequency of

910 resampled differences of the means that were greater than the observed.

911 **Figure 9.** Model of Ds activity and planar cell polarity in the larval ventral

912 epidermis. The strong Ds accumulation on both sides of T3 tendon cells (**figures**

913 **3, 4**) suggests that *ds* expression is high in T3 itself and/or its neighbours. In

914 addition, D::EGFP clones (**figures 5**, **6**) and ectopic denticles (**figure S3A**) show

915 that polarity of row 10 points backwards, away from T3, implying that Ds activity

916 is higher in row 11 than in T3. These two observations combined argue that *ds*

917 expression peaks in row 10, two cells anterior to the A/P border, with Ds activity

918 also high in T3 and row 11. Graded *ds* expression forwards and backwards from

919 this peak together with high levels of *fj* expression in tendon cells determine the

920 landscape of Ds activity, now extended to the undenticulate region. The Ds

921 gradient indicated has not been confirmed, it is a speculation. Our data suggest,

922 that if there is a pervasive gradient, it will be shallow, perhaps even more

923 shallow than shown. The differences in Ds activity between each cell's anterior

924 and posterior sides orient D accumulation; D localises to the side that has the

925 highest Ds activity and "sees" the lowest Ds activity in its neighbour. D

926 asymmetrical distribution precisely matches the pattern of cell polarity revealed

927 by denticles, as demonstrated by direct visualisation of tagged D in the whole

928 segment and induction of denticles in normally naked cells. Cell 11 is shown with

929 some ambiguity, because that is what we find (see main text). Blue shading

930 indicates P compartment cells, grey shading tendons.

931 **Movie 1**. Film of microtubule dynamics in a representative larval A cell. EB1::GFP

932 comets in a row 7 cell from the right hemisegment imaged for 4 minutes at 5.16s

933 intervals. Juxtaposed movie shows manual tracing of 200 comet trajectories over the

934 entire surface of the cell. Anterior is to the left, medial is down. Scale bar: 5**μ**m.

935 **Movie 2**. Film of microtubule dynamics in a representative larval P cell. EB1::GFP

936 comets in a row -1 cell from the left hemisegment imaged for 4 minutes at 5.16 s

937 intervals. Juxtaposed movie shows manual tracing of 200 comet trajectories over

938 the entire surface of the cell. Anterior is to the left, medial is up. Scale bar: 5**μ**m.

Table 1 Atypical cells: quantitation of predenticle polarities in relation to neighbouring cells, showing the effect of over expressing *ds* in the Tendon cells.

wild type

Anterior neighbour	Predenticle polarity of atypical Row 2 cells		Posterior neighbour
	Anteriorly	Posteriorly	
T1 cell	0	**44***	Row 3 cell
Row 2 cell	0	**52***	Row 3 cell

Predenticles of 39 atypical cells from 15 larvae. Fischer's exact test p-value = 1. *8 predenticles with an unclear position were allocated equally to these groups.

Anterior neighbour	Predenticle polarity of atypical Row 4 cells		Posterior neighbour
	Anteriorly	Posteriorly	
Row 3 cell	**207**	0	T2 cell
Row 3 cell	105*	**45**	Row 4 cell

Predenticles of 74 atypical cells from 21 larvae. Fischer's exact test p-value < 2.2^{-16}. *18 predenticles with an unclear position were arbitrarily added to this class, in favour of the null hypothesis.

sr.Gal4 UAS.EctoDs

Anterior neighbour	Predenticle polarity of atypical Row 2 cells		Posterior neighbour
	Anteriorly	Posteriorly	
T1 cell	**61**	8*	Row 3 cell
Row 2 cell	7**	**49**	Row 3 cell

Predenticles of 42 atypical cells from 28 larvae. Fischer's exact test p-value <2.2^{-16}. *6 and **3 predenticles with an unclear position were arbitrarily added to these classes.

| Anterior neighbour	Predenticle polarity of atypical Row 4 cells		Posterior neighbour
	Anteriorly	Posteriorly	
Row 3 cell	5	**119***	T2 cell
Row 3 cell	0	**99***	Row 4 cell

Predenticles of 40 atypical cells from 20 larvae. Fischer's exact test p-value = 0.068. *14 predenticles with an unclear position were allocated equally to these groups.
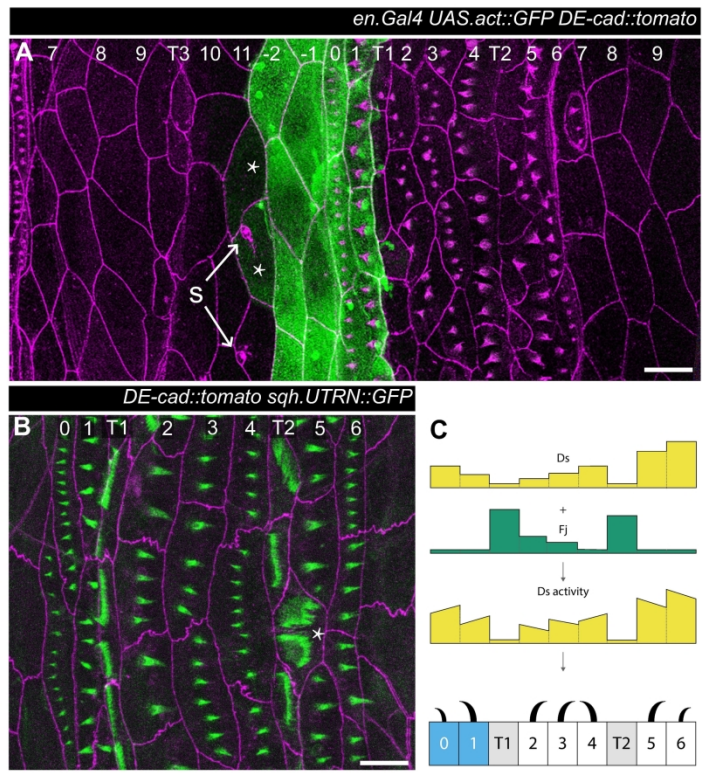
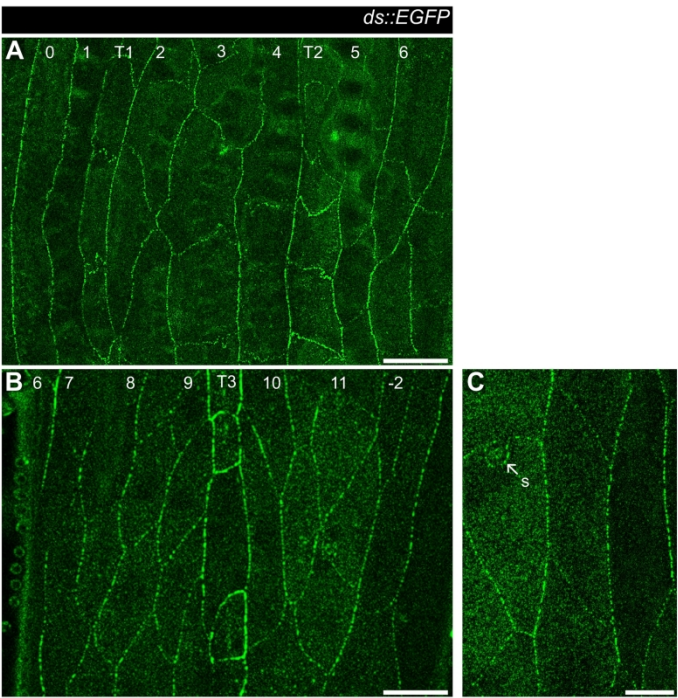Pietra et al. Figure 1

Figure 1

209x296mm (300 x 300 DPI)
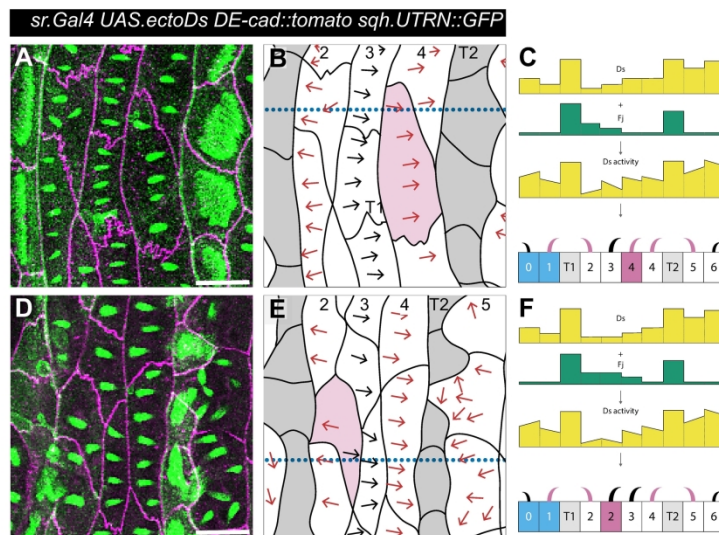
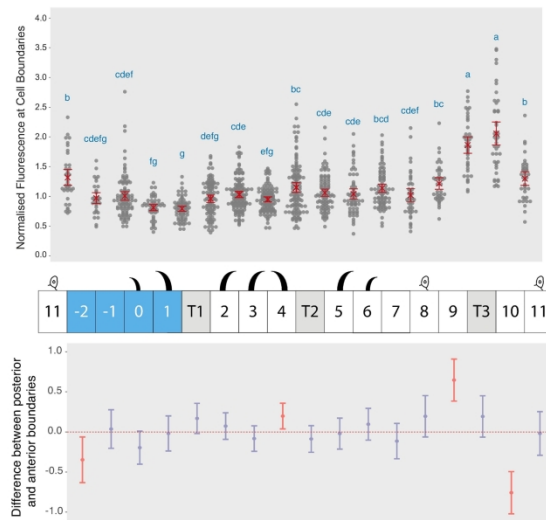Pietra et al. Figure 2

Figure 2

209x296mm (300 x 300 DPI)

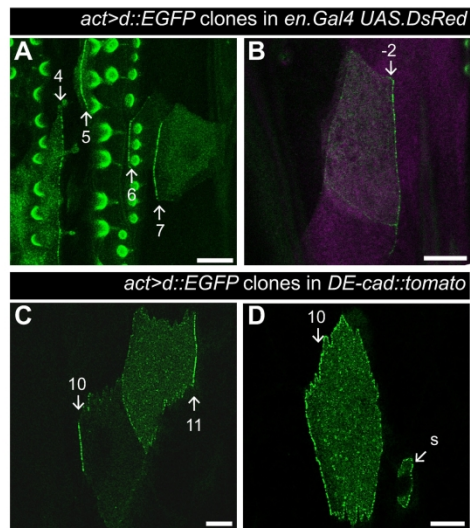Pietra et al. Figure 3

Figure 3

209x296mm (300 x 300 DPI)

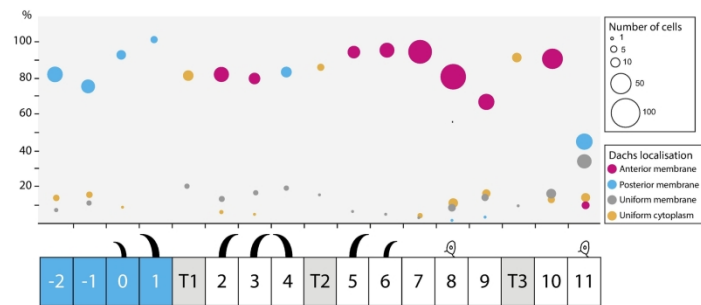Pietra et al. Figure 4

Figure 4

209x296mm (300 x 300 DPI)

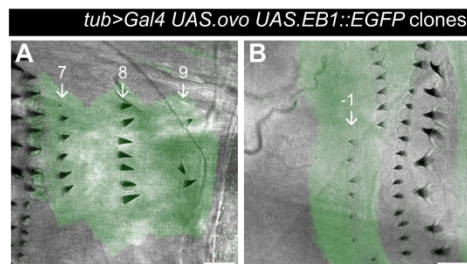Pietra et al. Figure 5

Figure 5

209x296mm (300 x 300 DPI)

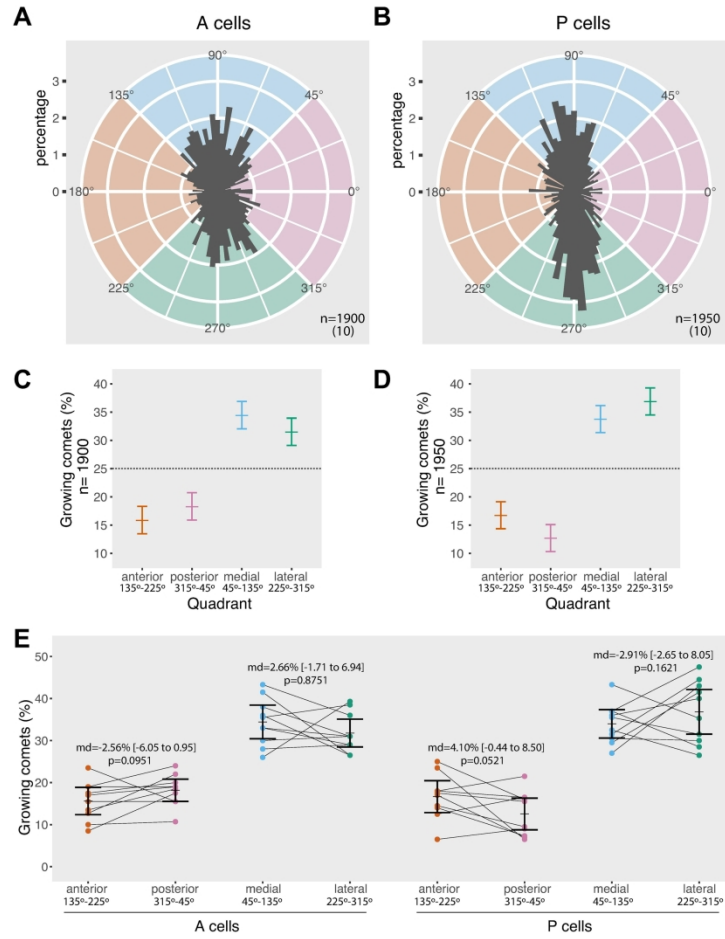Pietra et al. Figure 6

Figure 6

209x296mm (300 x 300 DPI)
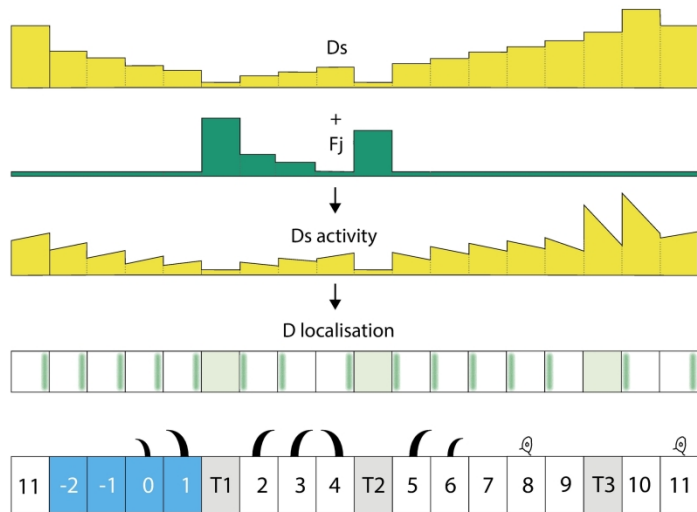
Pietra et al. Figure 7

Figure 7

209x296mm (300 x 300 DPI)

Pietra et al. Figure 8

Figure 8

209x296mm (300 x 300 DPI)

Pietra et al. Figure 9

Figure 9

209x296mm (300 x 300 DPI)